JOURNAL OF MATERIALS SCIENCE: MATERIALS IN MEDICINE **16** (2005) 417–421

Synthesis and structure of cerium-substituted hydroxyapatite

ZUDE FENG*, YINGMIN LIAO, MENG YE
Department of Materials Science and Engineering, State Key Laboratory of Physical Chemistry at the Solid Surfaces, Xiamen University, Xiamen 361005, China
E-mail: zdfeng@xmu.edu.cn

The aim of this study was to explore the effect of cerium ions on the formation and structure of hydroxyapatite (HAP). All particles, prepared by hydrothermal method, were synthesized at varied $X_{Ce} = Ce/(Ca + Ce)$ (from 0 to 10%) with the atomic ratio $(Ce + Ca)/P$ fixed at 1.67. Their morphology, composition and crystal structure were characterized by TEM, EPMA, XRD and FTIR. The results showed that in this composition range the apatite structure is maintained, Ce^{3+} ions could enter the crystal lattice of apatite and substitute Ca^{2+} ions. The doping of Ce^{3+} ions resulted in the decrease of the crystallite size with increase in X_{Ce}. The HAP particles without doping were short rods having a diameter from 10 to 20 nm and a length from 30 to 50 nm. They grew into long needles upon increasing X_{Ce}.

1. Introduction

Calcium hydroxyapatite ($Ca_{10}(PO_4)_6(OH)_2$, HAP) is the major inorganic components of human bone, dentine, and enamel. In biomedical application, HAP has been verified as a bioceramic having excellent biocompatibility and inductivity for bone ingrowth [1, 2]. The physical, chemical and biological properties of HAP were showed to be controlled by its crystal structure and composition. Accordingly, the substitution of Ca^{2+} with other metal ions affects important characteristics of HAP, such as crystallinity, solubility, thermal stability, metabolizability. Besides the reports regarding the substitution of Ca^{2+} ions by bivalent metals, the substitution of Ca^{2+} ion by trivalent metal ions attracted attention during the past few years [3–6]. Wakamura *et al*. indicated that Ca^{2+} ions of HAP were substituted by Cr^{3+} ions in one to one at $X_{Cr} \leq 0.13$ [3]. In another paper the same authors revealed that Fe^{3+}, Al^{3+} and La^{3+} could substitute Ca^{2+} ions through coprecipitation [4]. Besides, Ternane *et al*. reported the luminescence phenomena of a Eu^{3+} substituted calcium hydroxyapatite prepared by precipitation method [6]. However, according to the reports of these authors, as Cr^{3+}, Fe^{3+}, and Al^{3+} were doped into the HAP, structures other than HAP were detected, which meant that some of the doped metal ions did not enter the crystal lattice of HA [3, 4].

Decrease of the solubility of the mineral phases (mainly HAP) of teeth will aid in preventing caries. Therefore, significant effort has being implemented through decreasing the solubility of enamel at the surface of teeth. The study conducted by Bagam Bisa *et al*. suggested that rare-earth elements (for instance, lanthanum, cerium, etc.) might play an important role in enamel demineralization reduction [7]. Feng *et al*. indicated that the inhibitory ability of HAP on dissolution was improved significantly upon being treated in $CeCl_3$ solutions of concentrations above 100 ppm [8]. The phenomenon resulted from the formation of Ce-HAP. However, the detailed information relating the microstructure of Ce^{3+} doped HAP remains unclear.

The aim of this study was to explore the effect of Ce^{3+} ions on the formation and structure of hydroxyapatite (HAP). Since the radius of Ce^{3+} (1.01 nm) is close to that of Ca^{2+} (1.00 nm) [9], and the electronegativity of Ce^{3+} (1.06) is close to that of Ca^{2+} (1.04) as well, the effect of Ce^{3+} ions is supposed to differ from that of Cr^{3+}, Fe^{3+}, and Al^{3+}. To demonstrate this hypothesis, the morphology, composition and crystal structure of cerium substituted HAP were characterized by TEM, EPMA, XRD and FTIR. The noticeable influence of cerium ions on the crystal structure of HAP was discussed.

2. Materials and methods

The preparation of the particles was done by a hydrothermal method. Reagent grade $Ca(NO_3)_2$, $(NH_4)_2HPO_4$, and $Ce(NO_3)_3$ were used in this investigation. $Ca(NO_3)_2$ and $(NH_4)_2HPO_4$ were dissolved in deionized and distilled water. The mixing reaction was carried at 37 °C and under constant stirring. $Ce(NO_3)_3$ was added into the solution of $Ca(NO_3)_2$ and $(NH_4)_2HPO_4$ at different atomic ratios ($X_{Ce} = Ce/(Ce + Ca) = 0$–$0.1$) with the atomic ratio $(Ce + Ca)/P$ fixed at 1.67. The pH of the solution was adjusted

*Author to whom all correspondence should be addressed.

to 9.0 by an NH_4OH solution. The solution was then transferred into a capped Teflon vessel and aged at 100 °C for 8 h. After the aging the precipitates were filtered off, washed with deionized water and finally dried in a vacuum oven at 60 °C.

Morphology of the obtained particles was observed on a JEM100CX transmission electron microscope (TEM) after dispersed and ultrasonically treated in ethanol for 10 min. Crystal structure and cell parameters of the particles were characterized and analyzed using a X'Pert X-ray powder diffractometer (XRD) and attached software. The crystallite sizes of the particles were evaluated using the Scherrer equation from the half height width of the XRD peak at $2\theta = 25.8^\circ$ due to the (002) plane. Molecular structure of the particles was analyzed using a Nicolet Fourier transform infrared spectrometer (FTIR) by transmission method. For chemical composition analysis, particles were pressed in a steel mould to form disks of 2 mm in thickness and 10 mm in diameter. The uncoated disks were then placed onto a sample stage of a LEO-1530 scanning electron microscope and analyzed by an attached Cambridge electron probe microanalyzer (EDS). The SEM was operated at 20 KV and fast scan mode. Therefore, each result was an average of analytical area of 8 by 8 mm for all samples.

3. Results

Fig. 1 displays the morphology of HAP and cerium-substituted HAP particles. The HAP particles without doping are short rods having a diameter from 10 to 20 nm and a length from 30 to 50 nm (Fig. 1(a)). They grow into long needles upon increasing X_{Ce} (Fig. 1(b) and (c)). As $X_{Ce} \geq 0.07$, the diameter of the spiculate particles decreases to 3 to 5 nm, and the length of them increases to 100 to 150 nm.

Fig. 2 plots the energy dispersive spectrum of the particles of $X_{Ce} = 0.1$. The K and L characteristic peaks of cerium are quite obvious. In Fig. 3 Ca/P and (Ca + Ce)/P are plotted against X_{Ce}. Linear regression analysis shows a statistically significant decrease of Ca/P with the increase of X_{Ce} ($P = 0.001$), and no correlation existing between (Ca + Ce)/P and X_{Ce} ($P = 0.99$).

Fig. 4 shows that in the composition range of this study the apatite structure is maintained. There does not exist any noticeable diffraction peak other than HAP. Linear regression analysis shows that there does not exist any correlation between X_{Ce} and lattice constants (a and c) ($P_a = 0.996$ and $P_c = 0.990$, respectively) (Fig. 5). However, the intensity of XRD peak of (002) plane and the crystallite sizes of the particles decrease significantly upon increasing X_{Ce} at $X_{Ce} \leq 0.07$ (Fig. 6).

FTIR analysis indicates that no significant difference exists among the patterns of pure HAP and doped HAP (Fig. 7). The spectrum of the HAP particles shows the band at 3570 and 633 cm^{-1} due to the stretching and bending mode of OH^-, the bands at 1100, 1033 and 962 cm^{-1} due to the stretching mode of P—O, the bands at 602 cm^{-1} and 565 cm^{-1} due to the bending mode of O—P—O. Those are the major characteristic bands of HAP. Besides, a strong band at 1648 cm^{-1} and a broad band between 3000 and 3600 cm^{-1} present the existence of water molecular in samples. Compared to the spectrum of HAP, no significant shift either to lower or higher wave number is observed upon doping (Fig. 7(b)–(f)). These FTIR results are in good agreement with the XRD results.

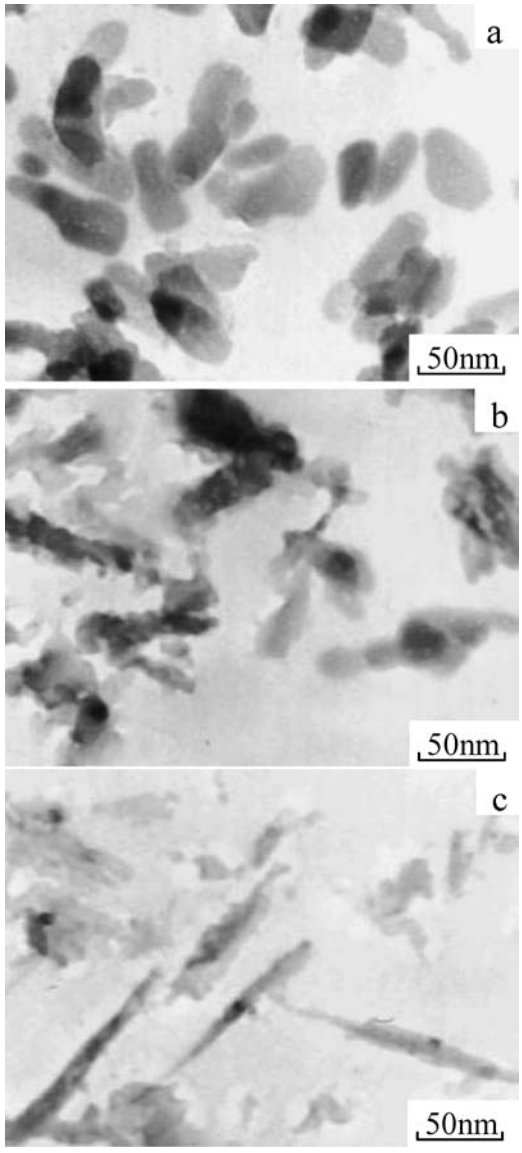

Figure 1 TEM pictures of the particles formed at varied X_{Ce}; (a) $X_{Ce} = 0$, (b) $X_{Ce} = 0.05$, and (c) $X_{Ce} = 0.07$.

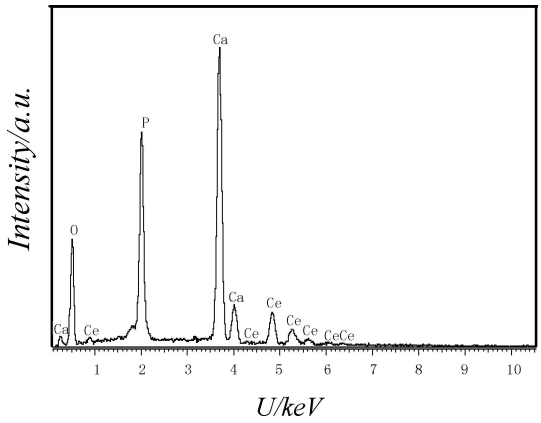

Figure 2 EDS patterns of the particles formed at $X_{Ce} = 0.1$.

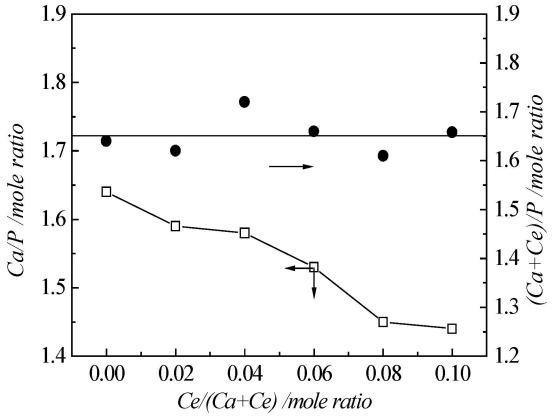

Figure 3 Ca/*P* (open symbols) and (Ca+Ce)/*P* (full symbols) of the particles formed at varied X_{Ce}.

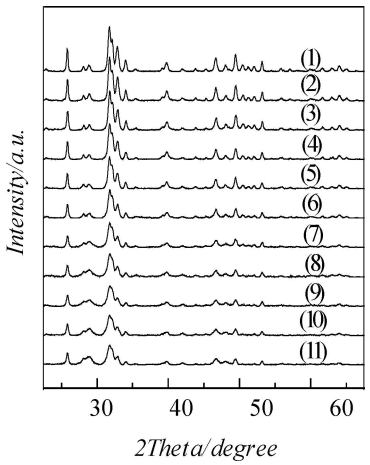

Figure 4 XRD patterns of the particles formed at varied X_{Ce}. (1) X_{Ce} = 0, (2) X_{Ce} = 0.01, (3) X_{Ce} = 0.02, (4) X_{Ce} = 0.03, (5) X_{Ce} = 0.04, (6) X_{Ce} = 0.05, (7) X_{Ce} = 0.06, (8) X_{Ce} = 0.07, (9) X_{Ce} = 0.08, (10) X_{Ce} = 0.09, and (11) X_{Ce} = 0.1.

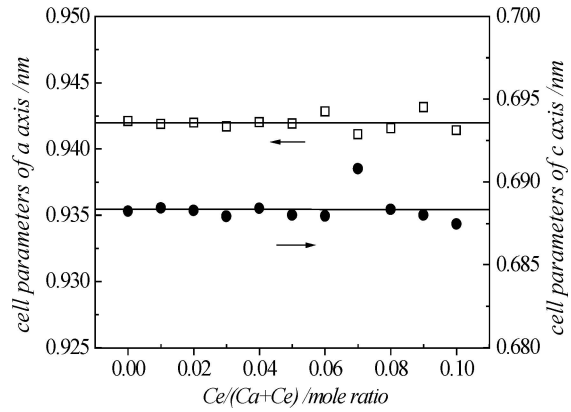

Figure 5 Evolution of cell parameters as a function of Ce content.

4. Discussion

As shown by XRD, FTIR, and EDX, within the range of X_{Ce} = 0–0.1 a single apatite phase was obtained. The analysis confirmed the substitution of Ca^{2+} with Ce^{3+} as well. In the study of Wakamura *et al.* they indicated that as Cr^{3+}, Fe^{3+}, Al^{3+} and La^{3+} were doped into the HAP, structures other than HAP were detected, which implyed that some of the doped metal ions might form compound instead of entry into the crystal lattice

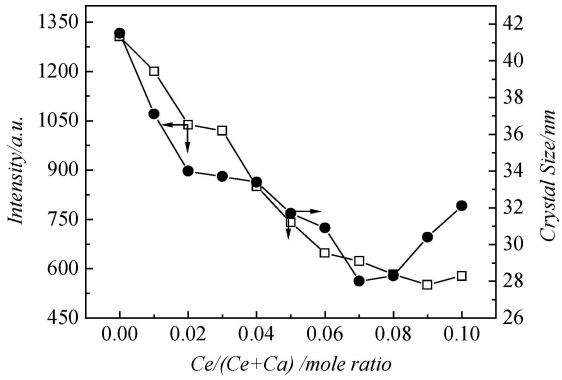

Figure 6 Intensity of XRD peak of (002) plane (open symbols) and crystal size (full symbols) of the particles formed at varied X_{Ce}.

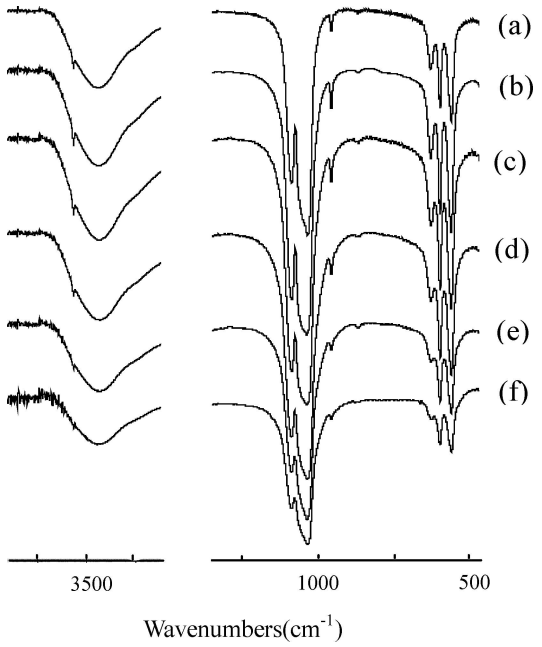

Figure 7 FTIR spectra of the particles formed at varied X_{Ce}: (a) X_{Ce} = 0, (b) X_{Ce} = 0.02, (c) X_{Ce} = 0.04, (d) X_{Ce} = 0.06, (e) X_{Ce} = 0.08, and (f) X_{Ce} = 0.1.

of HAP [3, 4]. Since the radius of Ce^{3+} (1.01 nm) is quite close to that of Ca^{2+} (1.00 nm), and the electronegativity of Ce^{3+} (1.06) is close to that of Ca^{2+} (1.04) as well, the behavior of Ce^{3+} ions in the crystal lattice of HAP is supposed to differ from that of Cr^{3+}, Fe^{3+}, Al^{3+} and La^{3+}. Due to the limitation of sensibility of XRD and FTIR, an EPMA (EDS) method was used to determine the chemical composition of the particles and double check the result. With the progress of hardware and software, the accuracy of quantitative analysis by EDX has been greatly improved during the past decade [10]. In addition, to improve the accuracy of EDS, several methods were practised during the analysis. Firstly, the particles were pressed into disks having smooth and flat surfaces to reduce the negative effect resulted from rough surface on the accuracy of measurement. Secondly, no coating was introduced during the analysis. Thirdly, fast scan mode was set during sampling to obtain an average based on an analytical area of 8 by 8 mm for each samples. Fourthly, the content of calcium, oxygen, phosphorus, and cerium in

the particles was much higher than the limitation of detection of EDS (0.2%), respectively. Finally, from the spectrums of EDX, no overlap of the characteristic peak, which was one of the major sources of inaccuracy, was found. The results of EDS analysis seem helpful (Fig. 3). Linear regression analysis shows a statistically significant decrease of Ca/P upon increasing X_{Ce} ($P = 0.001$), which suggests that Ca^{2+} in crystal lattice of HAP reduces with the increase of Ce^{3+}. Meanwhile, liner regression analysis shows that (Ca + Ce)/P keeps approximately constant ($\approx$1.67) in the range of $X_{Ce} = 0$ to 0.1 ($P = 0.99$), which implys that Ce^{3+} ions substitute the position of Ca^{2+} in the apatite lattice. Considering no existence of any noticeable diffraction peak and band other than that of HAP from XRD and FTIR analysis, the combining analysis of XRD, FTIR, and EDX confirm the substitution of Ca^{2+} in HAP with Ce^{3+}.

Cerium and calcium is a trivalent and bivalent ion, respectively. Therefore, the remarkable difference of valence of the two ions may introduce certain change of microstructure of Ce-HAP. This investigation detected several change of microstructure of cerium-substituted HAP. FTIR analysis indicates that no significant difference exists among the spectra of HAP and cerium-substituted HAP, and no significant shift either to lower or higher wave number was observed upon doping. However, the intensity of all bands is weakened upon increasing X_{Ce}. The weakening of OH-bands may be resulted from the breakage of balance of electric charge in HAP due to the substitution of Ca^{2+} with Ce^{3+}. In order to compensate these positive charges, OH^- may transform to O^{2-}, as suggested by Serret *et al*. [5]. The weakening of PO_4^{3-}-bands may arise from the introduction of Ce^{3+} and subsequent alteration of the bonding force between ions, which leads to the weakening of the vibration of P–O and O–P–O.

The intensity of diffraction peaks is weakened and half height width (HHW) of major diffraction peaks is widened upon increasing X_{Ce}. Two reasons may be responsible for the above phenomena. Firstly, the intensity of powder diffraction is affected by several factors such as crystal structure, species, number and array of atoms in cell, the integrality of the crystal, and the volume of crystal. The substitution of Ca^{2+} with Ce^{3+} results in the alteration of species of atoms in crystal cell and subsequent weakening of the intensity of diffraction. Secondly, the widening of HHW of diffraction peaks may result from distortion of crystal lattice or decrease of crystallite sizes. The study of Serret *et al*. showed that La^{3+} occupied the position of Ca^{2+} ions in apatite and induced the distortion of crystal lattice [5]. There existed a linear correlation between X_{La} and lattice constants (a and c). However, in this investigation, there did not exist statistical correlation between X_{Ce} and lattice constants according to regression analysis ($P_a = 0.996$ and $P_c = 0.990$). a and c were constant in the composition range. The difference observed in this study can be explained from the different atomic radii of lanthanum and cerium. The difference of the radius between Ca^{2+} and Ce^{3+} is negligible ($r_{Ca}^{2+} = 1.00$ nm, $r_{Ce}^{3+} = 1.01$ nm), and the electronegativity of Ce^{3+} (1.06) is close to that of Ca^{2+} (1.04). Therefore, the widening of diffraction peaks is supposed to be the result of the decrease of crystal size. According to the Bonn-Land formula, the lattice energy ($U = ANZ_1Z_2E_2/4\pi\varepsilon_0 r1$) is determined by the number of electric charge of ions. The greater the numbers of electric charge of the ions, the greater the lattice energy, which means the crystal is more stable. Since the number of electric charge of Ce^{3+} is greater than that of Ca^{2+}, Ce-HAP is more stable than HAP. During the process of nucleation, more nuclei may form in solution upon doping, which lead to the decrease of crystal size.

Another interesting result obtained in this study is the influence of cerium ions on the shape of particles. The crystallite size of HAP without doping nearly equals the length of the particles along c-axis of the crystal, which suggest particles being single crystal. However, original short rod-shaped particles grow into long needle-shaped particles upon increasing X_{Ce}. The result seems inconsistent with the XRD result that a decrease of crystallite sizes is obtained with the increase of X_{Ce}. The phenomenon suggests that the doped HAP particles are polycrystalline. Cerium may promote combination or connection of some crystallites along the c-axis direction to form needle-like particles. The study of Wakamura *et al*. had indicated that the substitution of Ca^{2+} in HAP with Cr^{3+} or Fe^{3+} would result in the acceleration of growth of HAP particles [4]. The results of this study coincide their results. However, the reason of this phenomenon remains unclear and further study is required.

5. Conclusions

Cerium substituted hydroxyapatite was prepared by hydrothermal method. In the composition range of X_{Ce} = Ce/(Ca + Ce) = 0–0.1 the apatite structure is maintained, Ce^{3+} ions could enter the crystal lattice of apatite and substitute Ca^{2+} ions. The doping of Ce^{3+} resulted in the decrease of the crystal's size with an increase in X_{Ce}. The HAP particles without doping were short rods having a diameter from 10 to 20 nm and a length from 30 to 50 nm. They grew into long needles upon increasing X_{Ce}.

Acknowledgments

The financial support from the State Committee of Development and Reformation is gratefully acknowledged.

References

1. R. GORCIA and R. H. DOREMUS, *J. Mater Sci.: Mater Med.* **3** (1992) 154.
2. C. K. HSU, *Mater. Chem. Phys.* **9470** (2002) 1.
3. M. WAKAMURA, K. KANDORI and T. ISHIKAWA, *Polyhedron* **16** (1997) 2047.
4. *Idem.*, *Colloids Surf.* **164** (2000) 297.
5. A. SERRET, M. V. CABANAS and M. VALLET-REGI, *Chem. Mater.* **12** (2000) 3836.
6. R. TERNANE, M. TRABELSI-AYEDI, N. KBIR-ARIGUIB and B. PIRIOU, *J. Luminescence* **81** (1999) 165.

7. F. B. BAGAM BISA, H. F. KAPPERT and W. SCHILI, *J. Oral. Maxillofac. Surg.* **52** (1994) 52.
8. Z. FENG, F. CHEN and C. J. LIN, *Chem. J. Chin. Univers.* **21** (2000) 298.
9. M. I. KAY and R. A. YONG, *Nature* **204** (1964) 1050.
10. L. Y. XU, Z. D. LIU and Y. H. SHANG, *Anal. Test. Techn. Instr.* **5** (1999) 115.
11. D. NICHOLAS, F. I. PRIEST and V. D. VYVER, in "Trace Metals and Fluoride in Bones and Teeth" (CPC Press Inc, 1990) p. 136.

Received 1 July
and accepted 1 November 2004